Divergence in the Pelagic Zone: Genomic Signatures of Speciation and Adaptation in the Ctenophore *Mnemiopsis*

Authors: Remi N. Ketchum[1,2*], Edward G. Smith[3], Leandra M. Toledo[1], Whitney B. Leach[4], Natalia E. Padillo-Anthemides[1], Andreas D. Baxevanis[5], Adam M. Reitzel[6], Joseph F. Ryan[1]*

Affiliations:

[1] Whitney Laboratory for Marine Bioscience, University of Florida, St. Augustine, Florida, USA

[2] Department of Genetics, University of North Carolina at Chapel Hill, Chapel Hill, North Carolina, USA

[3] School of Life Sciences, The University of Warwick, Coventry, UK

[4] Department of Biology, DeSales University, Center Valley, PA, USA

[5] Center for Genomics and Data Science Research, Division of Intramural Research, National Human Genome Research Institute, National Institutes of Health, Bethesda, Maryland, USA

[6] Department of Biological Sciences, University of North Carolina at Charlotte, Charlotte, North Carolina, USA

*Corresponding authors. Email: rketchum@ad.unc.edu, joseph.ryan@whitney.ufl.edu

Abstract

Background

Understanding how populations diverge is one of the most compelling questions in evolutionary biology but our grasp on the genomic mechanisms underpinning divergence is limited to a handful of species. Indeed, we know even less about divergence in the pelagic zone, where barriers to gene flow are seemingly absent. The holopelagic ctenophore *Mnemiopsis leidyi* is the most widely used ctenophore in experimental biology and has become an important model system in studies ranging from developmental biology to neurobiology. In addition, its relatively small and tractable genome provides a powerful foundation for genomic and evolutionary analyses. However, we still lack a clear understanding of species boundaries, population structure, and the evolutionary forces shaping divergence within *Mnemiopsis*, limiting both evolutionary and ecological interpretations. To expand our general understanding of divergence across novel environments as well as resolve a long-standing taxonomic debate, we generated the most comprehensive genomic study to date of the holopelagic ctenophore *Mnemiopsis* across a large expanse of its native range.

Results

By leveraging multiple analytical approaches and generating two near-chromosome level genomes, we identify two distinct species of *Mnemiopsis* with high levels of genome-wide divergence along the US Atlantic coast, which correspond to *M. leidyi* and *M. gardeni*. Our demographic analyses suggest that *M. leidyi* and *M. gardeni* began to diverge during the mid-to-late Pleistocene climate transitions and were later shaped by post-glacial oceanographic changes. We highlight substantial genomic rearrangements and copy number variation between species as well as uncover key genes under selection that are likely important for environmental adaptation.

Conclusions

Together, these findings provide compelling evidence that the ctenophore currently recognized as *M. leidyi* represents more than one species. Recognizing cryptic species boundaries is critical for future study designs, environmental monitoring, and developing targeted management strategies. Altogether, we connect microevolutionary processes with macroevolutionary patterns and provide new insights into how ocean dynamics drive speciation and adaptation in pelagic ecosystems.

Keywords: *Mnemiopsis,* pelagic invertebrate, structural variation, speciation, population genomics

Background

Speciation, the process through which populations diverge into groups that no longer exchange alleles [1], is a fundamental evolutionary process responsible for generating much of the biodiversity on earth. Understanding how populations diverge and eventually become reproductively isolated has been a central question in evolutionary biology for decades [2–4]. Two primary models have traditionally been invoked to explain this process. In the first, allopatric speciation, geographic barriers restrict gene flow, allowing populations to diverge independently. In the second, which includes parapatric and sympatric speciation, divergence occurs despite partial or complete geographic overlap [5, 6]. Although allopatric speciation is widely regarded as the predominant mode of speciation [3, 5, 7], its prevalence in marine environments is questionable given the scarcity of physical barriers and the high dispersal potential of many organisms, which can lead to patterns of extensive connectivity [8–11]. Indeed, understanding how species arise and become established is particularly challenging in marine environments, although many examples of coexisting marine sibling species suggest that marine speciation may often be sympatric. This

process could be driven either by rapid adaptation to different ecological niches, genomic features that limit recombination and restrict introgression at specific loci (termed barrier loci; [12–15]), and/or hidden barriers to gene flow. While the development and spread of incompatible genotypes is central to both sympatric and allopatric speciation, the exact genomic regions and architecture which mediate this incompatibility, and the chronology of these genetic changes is still widely debated [11, 16].

The genomic patterns associated with speciation depend largely on whether divergence happens in the presence or absence of gene flow, either during the initial split or following secondary contact [12, 17, 18]. In allopatric speciation scenarios, divergence can proceed unfettered by the homogenizing effects of migration [18, 19]. Meanwhile, in speciation-with-gene-flow scenarios, divergence is constrained by the balance between the degree of genetic linkage and recombination versus the strength of selection or drift [17]. In this scenario, regions of low recombination (e.g., centromeric regions or structurally complex loci), can facilitate divergence by maintaining linkage among locally adapted alleles despite ongoing gene flow [20, 21]. In marine species where physical barriers to dispersal can be weak, genomic features which reduce recombination are likely strong drivers of genomic divergence. However, most studies to date have focused on single nucleotide polymorphisms (SNPs) and while informative, this has left the contribution of structural variants to speciation comparatively unexplored (although see [6, 20–23]). Structural variants (SVs – insertions, deletions, and other genomic changes affecting >50 bp) can occupy more of the genome than SNPs, have the potential to dramatically change phenotypes, and are often more likely to impact organismal fitness than SNPs because they are big enough to contain entire genes and other functional elements [21, 24]. SVs have been shown to lead to reproductive isolation through several mechanisms [25], including: underdominance of

92 heterokaryotypes [26], suppression of recombination [27, 28], gene duplications causing intrinsic
93 postzygotic isolation [29], and SVs acting as mutations of large effect [21]. Despite their potential
94 to drive speciation, structural variants have remained understudied due to challenges in detecting
95 and genotyping them with short-read sequencing [30]. Recent methodological advances, however,
96 now enable the generation of chromosomal- or near-chromosomal-level genome assemblies,
97 providing new opportunities to comprehensively investigate SVs and their evolutionary
98 significance to speciation [12].

99 In addition to methodological biases, the vast majority of speciation literature is based on
100 terrestrial species with small population sizes, clear physical barriers to gene flow, and internal
101 fertilization, all traits which are expected to facilitate the emergence of reproductive isolation [31–
102 33]. To fully understand the mechanisms driving speciation, we must broaden the range of studied
103 organisms to include animals with diverse life history strategies, particularly pelagic invertebrates
104 that spend their entire life in the water column and are characterized by high fecundity [34], large
105 population sizes [35], and high dispersal potential. These traits are expected to produce weak
106 genetic differentiation and promote panmixia [36] and indeed, this pattern is observed in many
107 marine species [37–40]. Holopelagic species, such as *Mnemiopsis* (A. Agassiz, 1865), remain
108 particularly understudied in this regard.

109 *Mnemiopsis* is a genus within the phylum Ctenophora with a native range that extends
110 continuously along more than 25,000 km of the Atlantic coast of the Americas, from Kittery,
111 Maine to the Valdes Peninsula in Argentina [41–43]. These comb jellies are considered to be one
112 of the 100 most invasive species in the world [44] and their introductions into European waters
113 have triggered community trophic cascades and collapse of fisheries [45]. The extensive
114 geographic distribution and invasive abilities of *Mnemiopsis* are driven in part by its broad

115 environmental tolerance [46], flexible planktivorous diet [47], extensive regeneration abilities
116 [48], high fertility levels [49], and a capacity for self-fertilization [50]. Risk management for
117 invasive species requires genetic information to establish management units and accurate
118 taxonomic classification is a fundamental component of effective control measures. Further, many
119 invasive species have the capacity for rapid adaptation [51] which, in turn, may make them more
120 likely to speciate following a biological invasion although relatively few studies have examined
121 this phenomenon [52].

122 Despite its rich 100-year history as an evo-devo model [53] and the availability of extensive
123 genomics resources [54–57], our understanding of species boundaries in *Mnemiopsis* is subject to
124 debate [58–62]. The World Register of Marine Species (WoRMS) currently divides *Mnemiopsis*
125 into two accepted species: *Mnemiopsis leidyi* (A. Agassiz, 1865; type location Massachusetts) and
126 *Mnemiopsis gardeni* (L. Agassiz, 1860; type location South Carolina). A third species, *Mnemiopsis*
127 *mccradyi* (Mayer, 1900; type location South Carolina), is currently recognized as a synonym for
128 *Mnemiopsis leidyi* [63]. However, there is much confusion as to the ranges and differences in
129 morphology between these two named species which is further complicated by anthropogenic
130 range expansion. Most modern literature considers all ctenophores along the Atlantic and Gulf
131 coasts of the United States as a single species, specifically *Mnemiopsis leidyi* [64]. Earlier studies
132 have raised the possibility of multiple *Mnemiopsis* species [58–62], but the molecular data
133 available at the time were limited in either marker number or population sampling, making it
134 difficult to resolve this question conclusively. With the compact genome of *Mnemiopsis* and the
135 rapid democratization of next-generation sequencing (NGS) technologies, we can now examine
136 population relationships at unprecedented resolution and address this long-standing controversy
137 more comprehensively than was previously possible.

We conducted whole genome short read sequencing of 118 individuals from 13 populations within *Mnemiopsis'* native range along the United States Atlantic coast and generated two near-chromosomal length genome assemblies of a northern and southern representative of each genus. We applied a suite of genomic approaches to understand holopelagic population dynamics, demographic histories, changes in genomic architecture, and adaptation to new environments. Taken together, these findings highlight barriers to gene flow in holopelagic species, illuminate mechanisms that may underlie invasion success, and address a critical knowledge gap in marine speciation research, which has historically focused on a relatively narrow subset of species.

Results and Discussion

Whole-genome sequencing of Mnemiopsis populations

We collected and sequenced the genomes of 118 *Mnemiopsis* individuals from 13 populations from their native range along the US Atlantic coast (Figure 1A, Additional file 1: Table S1). All samples were collected from < 10m surface waters and preserved in ethanol within an hour of collection. We generated a total of 730 Gb of Illumina reads and an average genome depth of 18.89x. This sequence data was used to generate datasets for subsequent genomic analyses (see Methods).

We also produced two high-quality, near chromosome-level genome assemblies of one sample from Massachusetts (*M. leidyi*; northern lineage) and one sample from Florida (*M. gardeni*; southern lineage) using PacBio HiFi sequencing technology (Additional file 1: Table S2). When assembled, the *M. gardeni* genome was 206.6 Mb in length, with half of the genome assembled into contigs 3.6 Mb or larger (N50). The *M. gardeni* assembly was comprised of 174 contigs, with

161 the 100 largest contigs making up 98% of the assembly. The *M. leidyi* genome was 215.8 Mb in
162 length, with half of the genome assembled into contigs 2 Mb or larger. The *M. leidyi* assembly was
163 comprised of 207 contigs, with the 100 largest contigs making up 89% of the assembly. We
164 identified 27,570 and 26,046 protein-coding genes within the *M. gardeni* and *M. leidyi* genomes,
165 respectively, and were able to functionally annotate 27,476 genes within the *M. gardeni* genome
166 (Additional file 2: Table S3). Analyses using the Benchmarking Universal Single-Copy Orthologs
167 program [65] revealed that our assemblies exhibit a similar degree of completeness to other
168 ctenophore genomes ([54, 66], (Additional file 1: Table S2). We recovered 91% (83% complete
169 and 8% partial) of the expected core genes for *M. leidyi* with 9% of them missing. For *M. gardeni*,
170 we recovered 92% (84% complete and 8% partial) of the expected core genes, with 8% of them
171 missing.
172
173 *Population genomic evidence of two Mnemiopsis species*
174 We performed phylogenetic analyses using nuclear and mitochondrial markers from our
175 *Mnemiopsis* samples collected along the Atlantic Coast. Our nuclear phylogenetic tree (Figure 1B)
176 revealed the presence of two distinct clades that corresponded to the northern lineage (Woods
177 Hole, MA to Roanoke Island, NC) and the southern lineage (Pivers Island, NC to Panacea, FL).
178 We observed a similar two-clade pattern in our phylogenetic analysis of the complete
179 mitochondrial genomes (published mitogenome is 10,326 bp [67]), driven largely by ~100 nearly
180 fixed nucleotide differences (Figure 1C). However, we identified six individuals from populations
181 near the geographic interface of these two clades that exhibit mitonuclear discordance.
182 Specifically, we observed one individual collected at Gloucester Point, Virginia (VAV10) and four
183 individuals collected in Roanoke Island, North Carolina (NCX3–5,8) that had northern nuclear

184 and southern mitochondrial genotypes. Likewise, we observed one individual collected from
185 Wrightsville Beach, North Carolina (NCW15) that had a southern nuclear and northern
186 mitochondrial genotype. This level of mitonuclear discordance could be consistent with
187 hybridization in a secondary contact zone and early generation hybrids [62, 68].

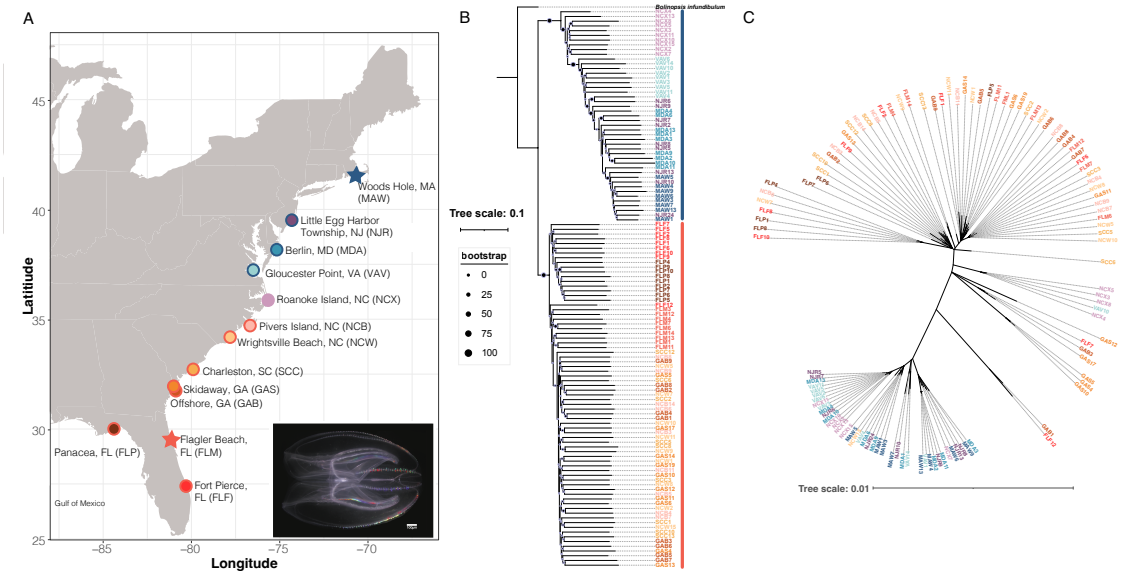

188

189 **Fig. 1. Mitonuclear discordance in *Mnemiopsis*. A)** Sampling map showing all *Mnemiopsis* collection
190 sites (site abbreviations in parentheses). The outer circle indicates the lineage assigned to each population
191 (blue = northern; red = southern). Roanoke Island, NC is shown without an outer ring because it is later
192 identified as a hybrid population. Stars denote populations also used for long-read PacBio HiFi genome
193 sequencing and assembly. **B)** Nuclear phylogeny inferred from 1,302 SNPs using ngsDist and FastME,
194 rooted with *Bolinopsis infundibulum*. Circle size at each branch reflects bootstrap support; both the northern
195 and southern lineages showed 100% support. Sample ID colors correspond to sampling locations (matching
196 panel A), and the colored bars to the right of each ID denote lineage membership (blue = northern; red =
197 southern). **C)** Mitochondrial phylogeny generated from a whole-mitogenome alignment using IQ-TREE
198 v2.3.2. Sample ID colors indicate lineage assignment.
199

200

201 To further investigate these admixture patterns, we evaluated the presence of 2–7 populations (by
202 adjusting the K parameter) within our dataset using ngsADMIX [69]. Setting K=2 separates
203 individuals into northern and southern lineages with the Roanoke Island, NC (NCX) and

204 Gloucester Point, VA (VAV) samples showing signs of admixture (Figure 2A). When K=3, the
205 Roanoke Island samples form their own subpopulation and, at higher K values, more substructure
206 within the two lineages becomes evident (Additional file 1: Fig. S1). MDS plots (Figure 2B)
207 support the results obtained using ngsADMIX, with the first principal component congruent with
208 the patterns observed by setting K = 2 and accounting for 39.4% of the variance in the data. The
209 average F_{ST} between the northern and southern lineage was 0.278 when Roanoke Island, NC was
210 included in the northern lineage, and 0.315 when it was removed from the comparison. Our
211 pairwise F_{ST} comparisons also highlight two distinct lineages (Additional file 1: Table S4). Due to
212 these cumulative results, we also tested for evidence of hybridization in our data using f_3 statistics
213 [70]. We compared the Roanoke Island, NC (NCX) population to the most northern population
214 (Woods Hole, MA; MAW) and most southern population (Panacea, FL; FLP) and, notably, this
215 resulted in a negative $f3$ statistic and an absolute Z score >= 3 (threshold used for significance),
216 highlighting a significant degree of admixture in the Roanoke Island, NC population (Additional
217 file 1: Table S5). In line with a recent study which detected evidence of admixture in Virginia [62],
218 we also observed signatures of admixture in Virginia (Gloucester Point, VA; VAV), as well as
219 other northern populations (including in populations ~450 km away, namely NJR and MDA). In
220 contrast, there is no admixture observed in any populations south of Roanoke Island, even though
221 Pivers Island, NC (NCB) is comparatively close (~180 km south).
222
223 Our analyses reveal two divergent genetic lineages in US Atlantic *Mnemiopsis*. These results are
224 consistent with previous studies that reported genetic differentiation between Massachusetts and
225 Florida populations [58] and identified a population breakpoint near Cape Hatteras, NC [59].
226 Building on this earlier work, our high-resolution spatial and genomic sampling further

227 demonstrates that the genetic breakpoint between the two lineages is a narrow hybrid zone. There
228 is cumulative evidence of admixture observed from Roanoke Island, NC up to Gloucester Point,
229 VA (~170 km north) but little evidence of admixture observed at Pivers Island, NC, which is
230 located only ~180 km to the south. Although *f*3-statistics suggest evidence of admixture in Little
231 Egg Harbor Township, NJ (NJR), and Berlin, MD (MDA), this result contrasts with the other
232 population genetic results and is therefore more likely explained by a counterintuitive property of
233 *f*-statistic computations known as sister repulsion [71]. Sister repulsion can occur when there is
234 unidirectional gene flow between study regions or when populations experience gene flow from
235 an unsampled genetically distant source. Extending our approach to new geographic locations
236 across the reported range of *Mnemiopsis* would make discerning between these two processes
237 possible. However, we posit that this pattern is most likely explained by unidirectional gene flow
238 given our demographic modeling results (see next section). Taken together, our findings indicate
239 that the genetic breakpoint is located where the Gulf Stream leaves the coast and moves offshore
240 into the open Atlantic Ocean, and we find evidence of a hybrid zone potentially resulting from
241 recent secondary contact. We also see high levels of genome-wide divergence, which tends to be
242 more typical of species that experienced geographic isolation during the early stages of speciation
243 [72, 73], however demographic analyses are required to explore this further. With this in mind, we
244 will hereafter refer to the northern lineage as *M. leidyi* and the southern lineage as *M.*
245 *gardeni* (following the naming scheme employed in WoRMS).
246
247

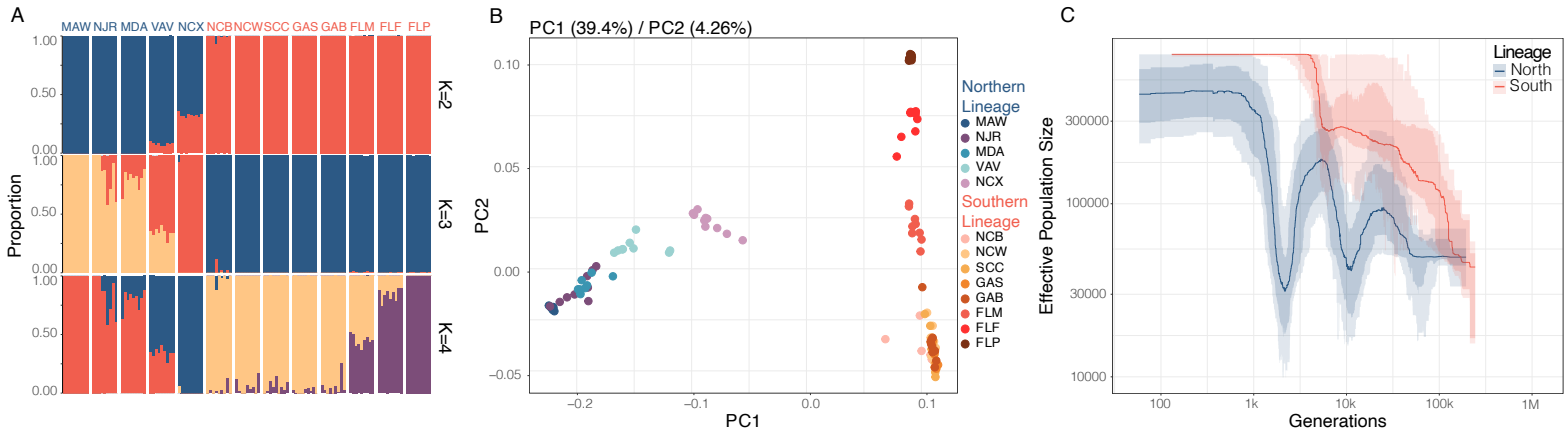

Fig. 2: *Mnemiopsis* exhibits strong population structuring along the US Atlantic Coast. A) Admixture plots for the 118 *Mnemiopsis* samples for K = 2 to K = 4 where each bar represents a single individual, and the colors represent each of the K components. **B)** MDS plot for PC1 and PC2 with the percent of total variance explained by each component shown above the plot in parentheses. Samples are colored according to their sampling location with *M. leidyi* samples (northern lineage) clustering on the left and *M. gardeni* samples (southern lineage) clustering on the right. **C)** Stairway plot results show different demographic histories of the two species with a generation time of one year and a mutation rate of 6.85 x 10^{-8} per base pair per year.

Demographic history of Mnemiopsis

We employed a Stairway Plot analysis [74] to reconstruct the demographic histories of *Mnemiopsis*, assuming a generation time of 1 year (see Methods). The two species show strikingly different population size trajectories beginning roughly 10,000 years ago (Figure 2C). Around this time frame, *M. gardeni* exhibits sustained population growth whereas *M. leidyi* displays a more complex history with two population bottlenecks, one around 10,000 years ago and a second between 2,000 - 3,000 years ago, followed by a recent recovery and expansion. The divergence between the effective population size curves for *M. gardeni* and *M. leidyi* that begins ~10,000 years ago coincides with major post-glacial events. Around this time, the Laurentide Glacier retreated (~8,000 years ago), and the sudden drainage of Lake Agassiz released a large influx of cold freshwater into the northern Atlantic [75]. This influx of cold freshwater likely reduced the

current in the ocean conveyor belt and resulted in a decrease in the amount of warm seawater traveling northward, subsequently causing temperatures to drop in the Northern Hemisphere [75, 76]. The population expansion that followed may have been a result of a reduction in the Gulf Stream current following the Lake Agassiz flood which would have allowed *Mnemiopsis* to migrate northward. It is unclear what would have caused the population bottleneck ~ 2,000 – 3,000 years ago in *M. leidyi*. It is possible that it was caused by the Little Ice Age – a cooling period in the northern hemisphere, although this occurred roughly between 1300 – 1850 [77, 78] and therefore does not line up perfectly with our estimated bottleneck.

Our results differ from the sequentially Markovian coalescent (PSMC) results reported in Jaspers et al. 2021 [58], which were based on a pairwise comparison of populations from Massachusetts and Florida. While both studies identify population expansions about ~50,000 generations ago and a population bottleneck ~10,000 generations ago, their *M. leidyi* samples did not show oscillating population size changes. Additionally, their *M. gardeni* samples showed a steady increase in population size from ~500,000-50,000 generations ago and then a decrease in population size from then onwards. In contrast, ours has shown a steady increase in population size from 100,000 generations ago to present day. The difference in findings can likely be explained by the increased geospatial resolution in our study. In addition, while the PSMC method [79] performs well for inferring ancient histories, the Stairway Plot method is more accurate for inference of more recent population histories and we see the greatest discordance in our results when looking at more recent population histories [74, 80].

292 Our demographic analysis using *Moments* further refined our understanding [81]. The best-fit
293 demographic model (sc3ielsm1, Additional file 1: Fig. S2-4) included secondary contact and three
294 epochs in each species following their initial divergence. The split between *M. leidyi* and *M.*
295 *gardeni* occurred approximately 223 Kya, followed by ~107 Kya of low-to-moderate bidirectional
296 gene flow. The second epoch began around 116 Kya and was characterized by genetic
297 isolation lasting roughly 89 Kya. The most recent epoch started approximately 27 Kya, during
298 which asymmetrical migration occurred predominantly from *M. gardeni* to *M. leidyi*. Across these
299 epochs, *M. leidyi* experienced an initial population expansion, followed by a sustained decline,
300 whereas *M. gardeni* displayed the opposite pattern, an initial contraction followed by consistent
301 population growth.
302

303 Together, Stairway Plot and *Moments* analyses reveal broadly consistent demographic patterns.
304 *Moments* infers a reasonably ancient divergence time, perhaps because incorporating migration
305 into the model allows some population differences to be explained by a more ancient split rather
306 than recent divergence. Both approaches recover evidence of pronounced population size
307 reductions in *M. leidyi*. The magnitude and number of contractions differ between methods, likely
308 because *Moments* is limited to modeling a maximum of three population size changes, whereas
309 Stairway Plot can recover more complex histories. These methods also concur that *M. gardeni* has
310 undergone a recent expansion, though they differ on whether *M. leidyi* has rebounded or continues
311 to experience a population contraction. Overall, the demographic models suggest that divergence
312 likely began in the mid-to-late Pleistocene, potentially caused by distant colonization events,
313 geological change, sea level changes or changes in prevailing currents [82]. However, it remains
314 unclear whether genetic isolation was initiated by glacially driven flooding and subsequent re-

strengthening of the Gulf Stream, or whether divergence predates these events, with post-glacial oceanographic changes instead facilitating secondary contact and asymmetric migration from *M. gardeni* to *M. leidyi*.

Structural genomic evidence of speciation

Chromosome-scale linkages of orthologous genes tend to be conserved even over very long time frames [83–87]. As such, chromosomal rearrangements are major evolutionary events that can either cause speciation events and/or provide evidence of long periods of isolation between lineages. To investigate structural differences between *M. leidyi* and *M. gardeni* genomes, we produced two high-quality, near chromosome-level genome assemblies of one *M. leidyi* sample from Massachusetts and one *M. gardeni* sample from Florida. We conducted macrosynteny analyses to check for evidence of chromosomal rearrangements between the two species' near-chromosomal length genome assemblies. In addition, we compared both genomes to the recently published chromosome-level genome assembly of *Bolinopsis microptera* [86], a lineage that is closely related to *Mnemiopsis* [88], in order to infer ancestral chromosomal states. We identified at least one chromosomal rearrangement between the *M. gardeni* and *M. leidyi* genomes (Figure 3A-C). The *M. leidyi* scaffold L006 maps to two *M. gardeni* scaffolds: G002, which maps completely to chromosome one of *B. microptera*, and G004, which maps completely to chromosome eight of *B. microptera*. The fact that this linkage group is present in both *M. gardeni* and *B. microptera* suggests that the genomic rearrangement occurred in *M. leidyi*. There are potentially other rearrangements involving the *M. leidyi* scaffolds L012 and L018, but a chromosome-scale assembly is needed to confirm or refute those possibilities.

338 As copy number variants (CNVs) can drive genome evolution [89] and contribute to both
339 speciation events [90] and environmental adaptation [91], we examined CNV patterns between the
340 two species. Genome-wide patterns of CNV across samples largely mirror that of SNP variation,
341 with separation of samples into clusters associated with *M. leidyi*, samples south of the Outer
342 Banks, and the Floridian samples (Additional file 1: Fig. S5). We assessed the 67 genes in the top
343 1% of fixation index values (V_{ST}; Additional file 3: Table S6). Of these 67 genes, only 21 (31%)
344 were assigned a gene ontology (GO) category [92] based on sequence similarity (Additional file
345 1: Table S7). We ran a Monte Carlo analysis and showed that this is significantly less ($P = 0.0006$)
346 than would be expected by chance. On average, a random set of 67 genes would produce 32 (48%)
347 genes within an associated GO category. These data suggest that the CNV outliers are enriched in
348 so-called "orphan" genes. This is not unexpected, as "orphan" genes are often associated with
349 effector functions (e.g., [93]) rather than highly conserved functions that are often critical to
350 survival.
351
352 The top V_{ST} CNV gene (jg9426 in the *M. gardeni* genome) is a putative G-protein coupled receptor
353 (GPCR), a class of cell surface receptors that detect molecules (e.g., light energy, lipids, proteins)
354 and activate cellular responses. This GPCR gene copy is missing from *M. leidyi* and appears to be
355 the result of either a species-specific duplication in *M. gardeni* or from a deletion of an ancestrally
356 duplicated gene in *M. leidyi* (*M. gardeni* gene IDs: jg9426 and jg9432, *M. leidyi* gene ID:
357 ML07987a; Figure 3D, Additional file 1: Fig. S6). It is one of four predicted GPCRs in these 67
358 genes (Additional file 1: Table S8). These GPCRs are all part of GPCR clades that have
359 independently radiated in ctenophores and have a many-to-many relationship with non-ctenophore
360 GPCRs, making it difficult to infer function. Loss or duplications in these genes would likely lead

361 to changes in sensory capabilities or cellular responses downstream of sensory inputs, changes that
362 are widely hypothesized to facilitate ecological speciation (speciation caused by divergent
363 selection; [94, 95]). These microevolutionary changes are consistent with the macroevolutionary
364 pattern of loss and expansion observed in GPCRs, offering insight into mechanisms that underly
365 the independent radiation commonly seen in phylogenetic analyses of channel and receptor genes
366 from multiple species. These observations are consistent with the "accordion model" of gene
367 evolution, where rounds of extensive loss are followed by rounds of extensive duplication [96].
368 Overall, patterns in the CNV data mirror those seen at the single nucleotide level and, although
369 gene loss in *M. leidyi* may be a result of severe bottlenecks or selective pressures, it may also stem
370 from reference bias, highlighting the need for pangenomic approaches [97, 98].
371
372
373
374
375
376
377
378
379
380
381
382
383
384
385
386
387
388
389

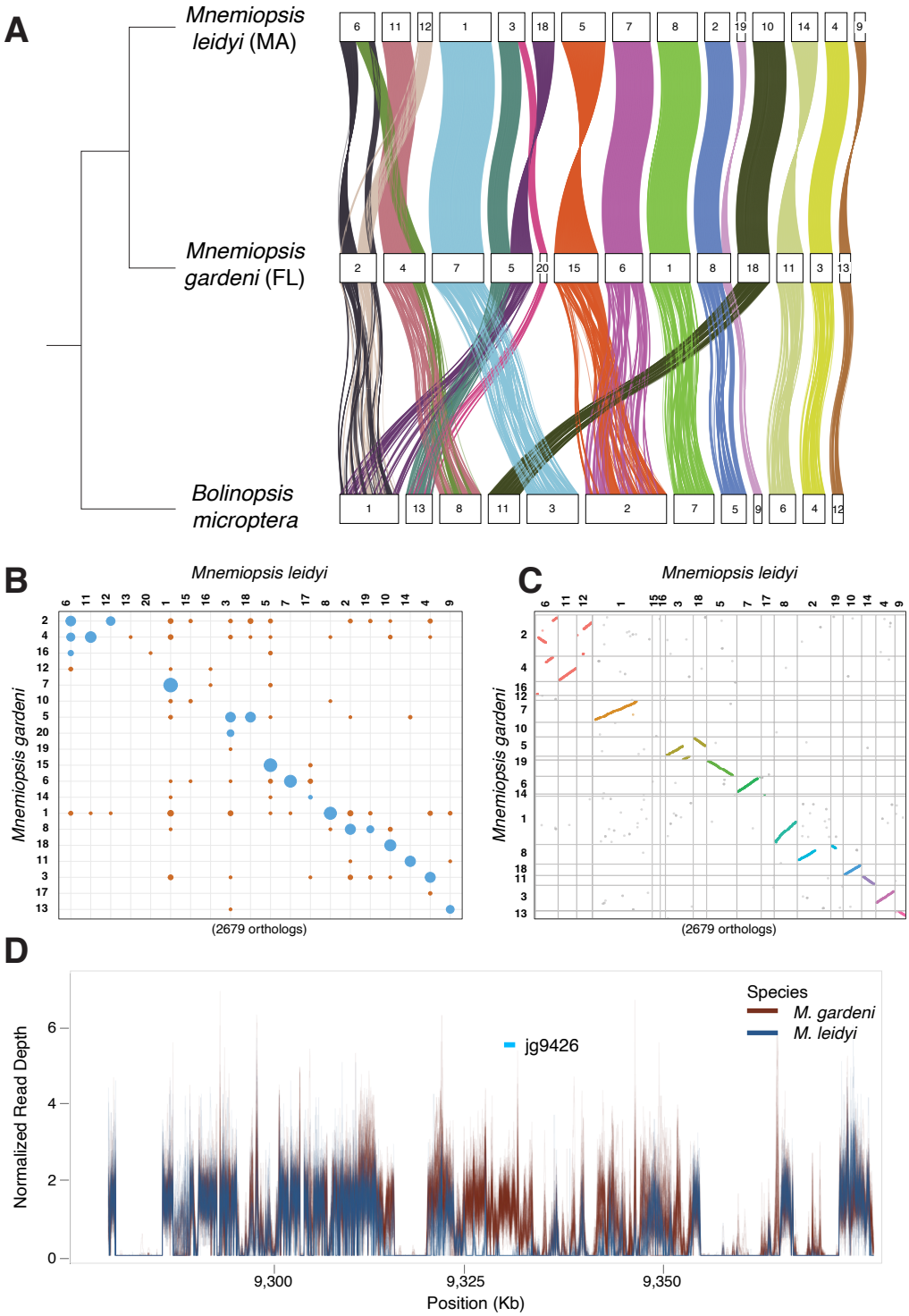

Fig. 3: Large-scale genomic rearrangements between species. (A) Chord diagram of macrosynteny on a near-chromosome scale between *Mnemiopsis leidyi* (top), *M. gardeni* (middle), and *Bolinopsis microptera* (bottom). The coordinates of 12,134 orthologs (based on reciprocal best BLAST hits) are plotted. **(B)** Plot of macrosynteny between *M. leidyi* and *M. gardeni*. **(C)** Oxford dot plot between *M. leidyi* and *M. gardeni*. Each dot represents an ortholog. **(D)** The genomic landscape neighboring the top copy

441 number variation outlier gene based on fixation index values (V_{ST}). Normalized read depth plot for short-
442 read sequences from *M. leidyi* (blue) and *M. gardeni* (red) for *M. gardeni* scaffold 001 from position
443 9,278,170 – 9,378,170.
444
445
446 *Genomic signatures of selection in genes mediating environmental sensing*

447 To investigate signatures of selection and local adaptation, we used the cross-population
448 composite-likelihood ratio (XP-CLR) test [99]. We observed key sensory related and neural genes
449 found in regions within the top 10% of XP-CLR values (Additional file 4: Table S9). These
450 included 79 GPCR's, four TRP channels, five glutamate receptors, the single *Mnemiopsis* voltage-
451 gated calcium channel, one of the two *Mnemiopsis* voltage-gated sodium channels, 10 voltage-
452 gated potassium channels, three acid-sensing ion channels (ASIC), two calcium-activated
453 potassium channels, a voltage-gated chloride channel, and a DEG/ENaC channel (Additional file
454 1: Tables S10-11). Our outlier dataset also contains many other genes that are relevant for nutrient
455 sensing and metabolism; these include the mechanistic target of rapamycin (mTOR), acetyl
456 coenzyme A synthase, malate dehydrogenase, and cytochrome c oxidase subunit 2 genes.
457

458 The top XP-CLR outlier region contains the *syntaxin-6* gene (jg7623), which promotes the
459 movement of transport vesicles to target membranes. We also observe the *O-GLcNAcase* (jg8681)
460 gene in the outlier dataset, which codes for a post-translational modifier of serine and threonine
461 residues on a wide range of proteins [100]. We highlight these two genes in Figure 4 as they have
462 both been implicated in modulating autophagic flux in response to nutrient status in
463 *Caenorhabditis elegans* [101, 102]. Both sweep regions show multiple signatures of selection,
464 including reduced nucleotide diversity in *M. leidyi*, elevated F_{ST} values, and an excess of rare
465 alleles (as evidenced by the more negative Tajima's *D* values for *M. leidyi*). We hypothesize that
466 overwintering in northern populations may be a driver of these selective sweeps, as organisms are

467 likely nutrient-deficient during this time. Interestingly, *M. gardeni* populations have significantly
468 lower Tajima's *D* values than *M. leidyi* populations across the entire genome (W=1.16 × 10^9; $P <$
469 0.01). However, this pattern breaks down at the target of selective sweeps. This may be consistent
470 with overall genomic patterns highlighting a population expansion in *M. gardeni* and population
471 contractions in *M. leidyi* that is disrupted at the site of selective sweeps.
472
473 To highlight functional categories of these genes, we conducted gene ontology (GO) analysis [92]
474 of the 2,093 genes that overlap with the genomic windows ranked in the top 10% of XP-CLR
475 values (Additional file 1: Table S12). These genes were significantly enriched ($P <= 0.05$) for GO
476 molecular function categories, including those associated with sensory processing, neural activity,
477 or diet, such as GPCR signaling pathways ($P = 0.0136$), GPCR activity ($P = 0.0152$), Golgi vesicle
478 transport ($P = 0.0399$), neurotransmitter transport ($P = 0.0424$), and chitin metabolic processes (P
479 $= 0.0056$). The chitin metabolic processes category includes two chitinase genes, which are critical
480 for digesting prey. These findings suggest that recent selection has acted on genes involved in
481 environmental sensing and resilience to nutrient deficiency and provide important candidate genes
482 for future functional verification.
483

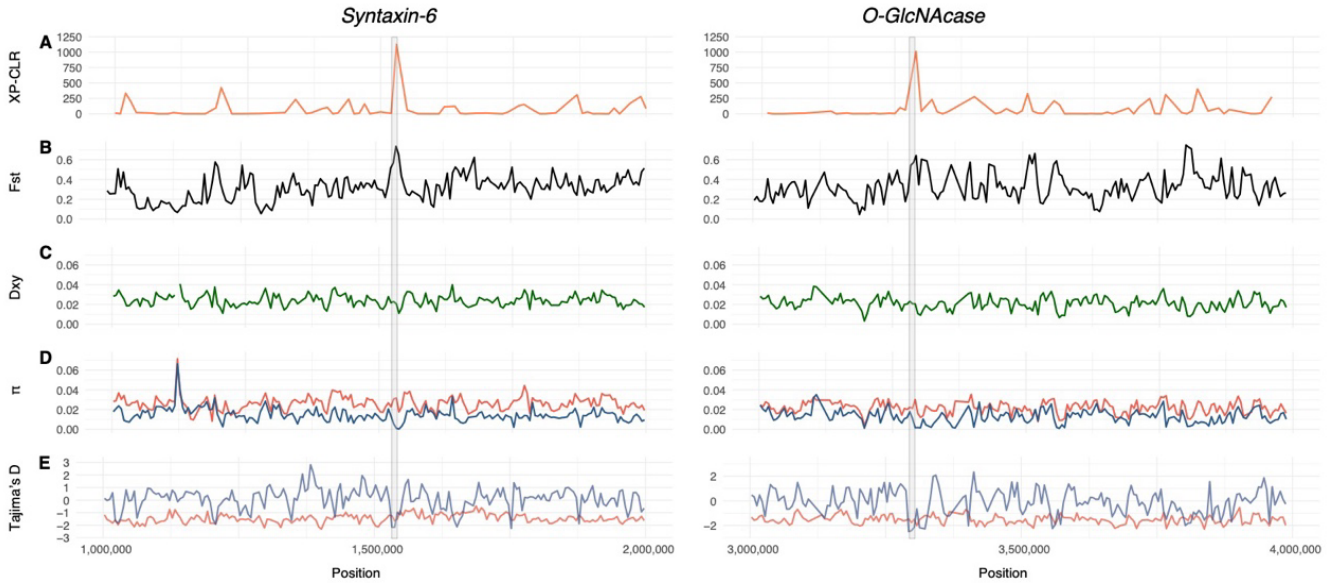

Fig. 4: **Genes involved in autophagic flux are under strong positive selection between species.** The two genes: *syntaxin-6* (left) and *O-GlcNAcase* (right) that are under putative positive selection. The (A) XP-CLR, (B) F_{ST}, (C) D_{XY}, (D) nucleotide diversity (π), and (E) Tajima's *D* values were calculated with nonoverlapping windows and step sizes. The locations of the two sweeping windows are shown with gray boxes. For panels D and E, blue lines indicate *Mnemiopsis leidyi* and red lines indicate *M. gardeni*.

Conclusions

Both the population genomic and structural genomic evidence are consistent with there being two species of *Mnemiopsis* on the US Atlantic coast. We report high levels of genome-wide divergence, as well as mitonuclear discordance. Demographic modeling suggests that these species diverged in the mid-to-late Pleistocene, with long-term genetic isolation followed by secondary contact and asymmetric migration from *M. gardeni* into *M. leidyi*, a scenario supported by the hybrid zone we identify along the North Carolina coast. We highlight large-scale genomic rearrangements between species that are consistent with a history of population contractions or small founder populations. We find evidence of selection on sensory and nervous system genes, with similar trends being reported in other species following speciation events [88, 103–106].

502 Further research is needed to investigate morphological, reproductive, and life-history traits that
503 may help provide further evidence for multiple species, as well as to examine the possibility that
504 more *Mnemiopsis* species exist in Central and South America, as the mitochondrial results of
505 Bayha et al. suggest [59]. More broadly, our knowledge of evolution is heavily biased across the
506 tree of life, and this study reinforces the importance of expanding taxon sampling as a means
507 towards gaining a much richer understanding of how evolutionary forces shape the genomic
508 variation between populations and species.
509
510 **Methods**
511 *Sampling*
512 One individual was collected from each of two locations for genome assembly: Woods Hole, MA
513 and Flagler Beach, FL. These samples were collected in August 2023 from surface waters (<2m)
514 using a cteno-dipper [49]. Samples were preserved in ethanol and placed in a -20°C freezer until
515 further processing.
516
517 A total of 118 *Mnemiopsis* samples were collected from thirteen locations along the Atlantic and
518 Gulf coast of the United States. These locations included: Woods Hole, MA, Little Egg Harbor
519 Township, NJ, Berlin, MD, Gloucester Point VA, Roanoke Island, NC, Pivers Island, NC,
520 Wrightsville Beach, NC, Charleston, SC, Skidaway Island, GA, Skidaway Island offshore, GA,
521 Flagler Beach, FL, Fort Pierce, FL, and Panacea, FL (Figure 1). Samples were collected between
522 August 2021 and November 2022 from surface waters (<10m) using either a cteno-dipper or a tow
523 net. Samples were immediately preserved in ethanol and placed in a -20°C freezer until further
524 processing.

525

526 *DNA Extraction and Sequencing*

527 High molecular weight DNA was extracted according to the CTAB/chloroform protocol detailed
528 in Erlich et al. 2017 [107]. DNA extractions were visualized on a 1% agarose gel for quality control
529 and quantified using a Qubit dsDNA High Sensitivity Assay Kit on a Qubit 2.0 Fluorometer. For
530 the genome assemblies, sequencing was performed on a Pacific Biosciences Sequel IIe platform,
531 in the Circular Consensus sequencing (CCS) mode. A total of 17.7 - 20.2 Gb of HiFi reads were
532 generated using CCS for the two individuals. PacBio library preparation and sequencing were
533 performed at NIH Intramural Sequence Center (NISC) in Rockville, MD.

534

535 For short-read whole genome sequencing, all DNA extractions were visualized on a 1% agarose
536 gel for quality control. One hundred and eighteen individually indexed, paired-end libraries with
537 an approximate insert size of 550 bp were constructed using the NEBNext Ultra II FS DNA Library
538 Preparation kit. Whole-genome sequencing was performed at the University of Florida's ICBR
539 Bioinformatics Core Facility on a single flowcell lane of a NovaSeq6000.

540

541 De novo *Genome Assembly*

542 Hifiasm v0.19.8 [108] was used to assemble the two genomes. For the Flagler Beach, FL
543 individual, the `--hom-cov` flag was set to 90. To reduce the amount of duplication,
544 PurgeHaplotigs v1.1.2 [109] was run with the 'contigcov' option for low coverage, low point
545 between the peaks, and high coverage cutoffs set to 10, 70, and 175 respectively. The percent
546 cutoff for identifying a contig as a haplotig (`-a` flag) was set to 50% and this assembly was
547 subsequently run through PurgeHaplotigs 'clip' option that identifies and trims overlapping contig

548 ends. For the Woods Hole, MA individual, the `--hom-cov` flag was set to 101, the 'contigcov'
549 options were set to 25, 70, and 155, and the `-j` and `-s` flags were both set to 55. The percent
550 cutoff `-a` flag was set to 60% and the final assembly was also clipped to remove overlapping
551 contig ends.
552
553 *Gene Prediction and Annotation*
554 Genomic repetitive elements were identified with RepeatModeler v1.0.11 [110] to generate a
555 *Mnemiopsis*-specific repeat element library. Repetitive regions were soft masked prior to gene
556 prediction and annotation using RepeatMasker v4.0.8. We aligned previously published bulk
557 RNA-Seq reads from tissues (PRJEB28334; [111]) to the above genome assembly using Bowtie2
558 [112]. Aligned RNA-seq data and gene models for *M. leidyi* (ML2.2.aa) were input into Braker
559 v2.1.5 [113]. Assembled gene/protein models were functionally annotated using BLASTP v2.9.0+
560 with three protein databases: UniProt Knowledgebase Swiss-Prot protein models v2021-03,
561 RefSeq invertebrate protein models, and the *M. leidyi* protein models [54]. Finally, BUSCO v5
562 [65] was used to measure the completeness of the genome assembly and protein sequences using
563 the Eukaryota database.
564
565 *Macrosynteny Analysis*
566 We analyzed conserved chromosome-scale synteny (macrosynteny) between these new Florida
567 and Massachusetts *Mnemiopsis* assemblies, as well as the published *Bolinopsis microptera*
568 genome assembly. To identify conserved genes, we performed diamond BLAST [114] to compute
569 the reciprocal best BLAST hits between the 2013 ML2.2 *Mnemiopsis* gene models and the gene
570 models of each of the new *Mnemiopsis* assemblies and the published *B. microptera* gene models.

571 These reciprocal best BLAST hits were used to identify significantly conserved macrosyntenic
572 blocks in MacrosyntR (version 0.3.3; [115]).
573
574 *Copy Number Analysis*
575 Copy number variation between the two species was assessed using the GATK germline CNV
576 (gCNV) pipeline in cohort mode [116]. The pipeline was run using the exome approach to focus
577 specifically on genic regions and gene intervals were padded by 250 bp. Intervals with fewer than
578 50 reads in greater than 50% of individuals were excluded and samples from Roanoke Island in
579 North Carolina were excluded due to their admixture. Denoised copy number ratios were
580 processed in R to remove copy number invariant loci, perform principal component analysis, and
581 to calculate the V_{ST} statistic. Loci with the top 1% of V_{ST} values were considered outliers.
582 Microsynteny plots for CNV loci were generated by performing contig alignments in MUMmer
583 [117]. SYRI was subsequently used to identify synteny and structural rearrangements, with plots
584 generated using Plotsr [118, 119] and read depth was calculated using Samtools v.1.9 [120].
585
586 *Data Processing and Filtering of Short-Read Data*
587 Raw sequence data was trimmed using Trimmomatic v0.39 [121] with a minimum phred score of
588 33. Once the data was filtered and adaptors were removed, the paired sequences were aligned to
589 the Flagler Beach, FL genome using BWA-mem v0.7.12 [79]. Sequence alignments were filtered
590 using Samtools for a minimum quality score of 30, Sambamba v0.6.6 [122] was used to filter
591 duplicate reads with default parameters, and bamutil v1.0.15 [123] was used to clip overlapping
592 read pairs.
593

594 We generated three datasets for our different analyses: LD-Filtered (89,750 SNPs), Lineage-
595 Specific Filtered (3.8 million SNPs), and the All-Sites Filtered (81 million positions). For each
596 dataset, we used the Flagler Beach, FL genome as our reference and ancestral genome as it was
597 the most contiguous assembly.
598
599 LD-Filtered Dataset. This dataset was produced by using ANGSD v0.921 [124] to call SNPs and
600 estimate genotype likelihoods using the Samtools model (`-GL 1`). We filtered the SNP data for
601 1) positions that were present in at least 94 out of 118 samples, 2) a maximum coverage of 2,360x
602 per site across all individuals to avoid calling sites in highly repetitive regions, 3) a minimum of
603 354x coverage per site across all individuals, 4) a minimum base quality score >20, 5) a *P*-value
604 cut off of 10^{-6} for calling polymorphic loci and 6) retained only SNPs with a global minor allele
605 frequency >5%. The ANGSD output was then subsampled for one SNP out of every 50 and
606 pairwise linkage disequilibrium (LD) was estimated with ngsLD v1.1.1 [125] on this subsampled
607 dataset. Linked sites were pruned with the script 'prune_graph.pl' with a maximum distance of 10
608 kb between SNPs and a minimum weight of 0.5 [126]. The final LD-Filtered dataset was used to
609 generate phylogenetic trees, ngsADMIX and MDS plots, and to calculate population pairwise F_{ST}
610 statistics.
611
612 Lineage-Specific Filtered Dataset. The second dataset was filtered using the same ANGSD flags
613 as the first dataset (excluding the LD filtering steps) but then underwent a second round of lineage-
614 level filtering. Specifically, sampling locations from Woods Hole, MA to Roanoke Island, NC
615 were included in the 'northern lineage' group and sampling locations from Pivers Island, NC to
616 Panacea, FL were included in the 'southern lineage' group. These two groups were filtered

separately and then later recombined. For the northern lineage, we filtered the dataset for 1) positions that were present in at least 36 out of 45 individuals, 2) a maximum coverage of 900x coverage per site across all individuals, 3) a minimum of 108x coverage per site across all individuals. For the southern lineage we filtered the dataset for 1) positions that were present in at least 58 out of 73 individuals, 2) a maximum coverage of 1,460x coverage per site across all individuals, 3) a minimum of 175x coverage per site across all individuals. We restricted the secondary lineage-specific filtering step to the subset of positions that were retained in the first round of filtering using the sites option in ANGSD. Filtering in this manner guarantees that sites with an allele that is fixed in one lineage will be retained. The final lineage-specific filtered dataset was used to generate sliding window F_{ST} values, XP-CLR values, and to calculate f_3 statistics.

All-Sites Filtered Dataset. The third dataset was filtered with the same method as the Lineage-Specific Filtered dataset, but we included all non-polymorphic sites. This dataset was used as input to our demographic analyses and to calculate nucleotide diversity [127], Tajima's *D* [128] and D_{XY} values.

Population Structure Analysis

We used the ngsDist option in ngsTools [129] on the LD-Filtered dataset to compute genetic distances between individuals and perform multiple dimensional scaling (MDS). We then looked for signatures of admixture using ngsADMIX [69] with runs ranging from K = 2 to K = 7. Weighted pairwise F_{ST} values were estimated between the individuals from the North (Woods Hole, MA to Roanoke Island, NC) and the individuals from the South (Pivers Island, NC to Panacea, FL) using ANGSD with the `-doSaf 1` flag. We then used realSFS to estimate the 2D

640 site frequency spectrum for each population and calculated the average pairwise weighted F_{ST}
641 using `realSFS fst`. Weighted pairwise F_{ST} estimates were also calculated between each
642 sampling location using ANGSD with the same parameters.
643
644 NgsDist was used to compute genetic distances from genotype probabilities with *Bolinopsis*
645 *infundibulum* as the outgroup (PRJNA818620; [86]). Raw *Bolinopsis* sequences were filtered
646 according to the same protocol as was applied to *Mnemiopsis* and then we ran ANGSD with
647 *Bolinopsis* included, a minor allele frequency filter of 0.05 and a SNP *P*-value cut off of $1x10^{-6}$.
648 This set of filters resulted in 1,302 SNPs that were used to generate the phylogenetic tree based on
649 the nuclear genome. NgsDist was run with 100 bootstrap replicates and a boot block size of 20.
650 Finally, FastME v2.1.6.1 [130] was used to visualize the pairwise genetic distances and RAxML-
651 NG v0.9.0 [131] was used to place bootstrap supports onto the tree. Final figures were generated
652 using the Interactive Tree of Life tool v6.9.1 [132].
653
654 Novoplasty v4.3.1 [133] was used to extract the mitochondrial genome from each trimmed sample
655 using the published *Mnemiopsis leidyi* COI sequence (KF435121.1 [134]) as the seed. When this
656 was unsuccessful, we instead used the published *Bolinopsis microptera* (PRJNA716277 [88])
657 whole genome sequences and ran Novoplasty with the published *B. microptera* COI seed
658 (MW735734.1 [135]) to extract the complete mitochondrial genome. The complete *B. microptera*
659 mitochondrial genome was then used as a seed for the remaining samples that initially failed
660 Novoplasty. Using this approach, we were able to successfully assemble 112 out of 118 complete
661 *Mnemiopsis* mitochondrial genomes. Next, we used MARS [136] to ensure that each
662 mitochondrial genome began at the same location using the branch and bound method and the

663 block length set to 100. We used MAFFT v7.480 [137] to generate an alignment and IQ-TREE
664 v2.3.2 [138] to generate a phylogenetic tree.
665
666 *Demographic Analysis*
667 To infer the demographic history of these species, we used two approaches based on allele
668 frequency spectra. First, StairwayPlot v2 [74] was used to reconstruct effective population size
669 estimates based on the folded SFS generated from the All-Sites Filtered dataset. Stairway Plot is
670 an unsupervised analysis method that does not require prespecified demographic models. We used
671 a mutation rate of 6.85×10^{-8} per base pair per year [58] and a generation time of 1 year [139]. The
672 hermaphroditic *Mnemiopsis* can reproduce within the first month of its lifespan [140], its lifespan
673 is approximately 2 years [139], and there is no information indicating that they ever lose the ability
674 to reproduce. As such, the mean age of reproduction was set to 1 year but due to the surrounding
675 uncertainty, we plotted the results in generations.
676
677 Second, we used the *Moments* Python library [81] based on the two-dimensional AFS to estimate
678 population size changes and the timing and magnitude of introgression between each pair of
679 genetic lineages. We subsampled our data so that we only included four populations, two *M. leidyi*
680 populations (Woods Hole, MA and Little Egg Harbor, NJ) and two *M. gardeni* populations (Fort
681 Pierce, FL and Panacea, FL), to conservatively remove putative hybrids and for computational
682 efficiency. This dataset returned approximately 21 million sites in total. Unlike the Stairway Plot
683 analysis, the *Moments* workflow requires demographic models to be specified at the start of the
684 analysis. Here, we explicitly tested 102 demographic models (described in detail at
685 https://github.com/z0on/AFS-analysis-with-moments/) that represent a wide range of possible

686 demographic histories. Following the *Moments* pipeline described in Rippe et al., 2021, we first
687 generated 100 bootstrapped two-population AFS datasets [141]. For a subset of 10 of these
688 bootstrapped AFS, each of the 102 models was run six times using randomized starting parameters.
689 Model log likelihoods were converted to Akaike's information criterion (AIC) which were then
690 used to find the best-fit run out of the six runs for each bootstrapped replicate. From the resulting
691 set of AIC values, the demographic model with the lowest median AIC value across all 10
692 bootstrapped AFS replicates was chosen. Finally, the 'winning' demographic model was fitted to
693 all 100 bootstrapped AFS to evaluate parameter uncertainties. As with the Stairway plot analysis,
694 we assumed a mutation rate of 6.85×10^{-8} per base pair per year and a generation time of 1 year.
695
696 *F_3 Statistics*
697 We used f_3 statistics, included as part of the ADMIXTOOLS package v.7.0.2 [70], as a test for
698 detecting hybridization. The f_3 statistic is a tool to test whether a population is admixed between
699 two source populations or to measure shared genetic drift between two test populations compared
700 to an outgroup population. If the f_3 statistic is negative, this suggests that admixture has likely
701 occurred. For this analysis, all populations which belonged to the northern mitochondrial lineage
702 were combined into one population and all the populations which belonged to the southern
703 mitochondrial lineage were combined into the second population. These two lineages were tested
704 against Roanoke Island, NC and Gloucester Point, VA.
705
706 *Genomic Signatures of Selection*
707 To detect regions of the genome under putative selection between the two lineages, we used XP-
708 CLR [99] which uses the AFS to calculate local deviations between populations. We used a sliding

window and step size of 10 kb with the `maxSNPs` flag set to 200. The genomic regions in the top 10% of the XP-CLR values were considered to represent selective sweeps and were associated with overlapping genes using Bedtools v.2.29.0 [142]. We used InterProScan (version 5.25-64) to associate gene ontology categories with the *M. gardeni* gene models. We conducted a Monte Carlo analysis to identify overrepresented gene ontology terms as was conducted in Babonis et al. 2018 [111].

To further characterize genomic patterns of regions under selection, we generated sliding window scans for F_{ST}, D_{XY}, nucleotide diversity (π), and Tajima's *D* values, with the hybrid Roanoke Island, NC population removed. The Lineage-Specific Filtered dataset was used to generate the F_{ST} values. We used `realSFS` F_{ST} `index` in ANGSD to compute per-site F_{ST} indexes and `realSFS` F_{ST} `stats2` to perform a sliding window analysis with the window and step size set to 5 kb to ensure nonoverlapping windows. The All-Sites Filtered dataset was used to generate nucleotide diversity, Tajima's *D,* and D_{XY} values. For nucleotide diversity and Tajima's *D* calculations, we used `realSFS saf2theta` in ANGSD to generate folded SFS's and then calculated these values along a sliding window (window size 5 kb, step size 5 kb) with `thetaStat do_stat`. For D_{XY} calculations, we used the CalcDxy.R code by Joshua Penalba in ngsTools [129] and then averaged the resulting values over the same 5 kb windows as the F_{ST} and nucleotide calculations. By combining several tests and summary statistics, we can make inferences about evolutionary forces acting on regions of interest with greater certainty.

Abbreviations:

SNP – Single Nucleotide Polymorphism

733 SV – Structural Variant

734 MDS – Multidimensional Scaling

735 PSMC – Pairwise Sequentially Markovian Coalescent

736 AIC – Akaike's Information Criterion

737 GO – Gene Ontology

738 COI – Mitochondrial Cytochrome C Oxidase subunit I

739 LD – Linkage Disequilibrium

740 CNV – Copy Number Variation

741

742 **Declarations:** ***Acknowledgements.*** We would like to thank Dr. Ann Tarrant, Roland Hagan,

743 Robert Aguilar, Dr. Deborah Steinberg, Tor Mowatt-Larssen, Eli at Outer Banks Kayaking

744 Adventures, Ken Song, Carol Smith, Dr. Joshua Osterberg, Dr. Jacob Warner, Dr. Daniel Sasson,

745 Dr. Marc Frischer, Dr. Adam Greer, Kyle Aaron, Dr. Holly Sweat, and Dr. Yuriy Bobkov for

746 help collecting *Mnemiopsis* samples along the US Atlantic coast. We also thank Dr. Dan

747 Schrider and Austin Daigle at UNC Chapel Hill for help analyzing and interpreting demographic

748 modeling results. We would like to acknowledge the ICBR for their excellent sequencing and

749 service (RRID:SCR_019152). We would like to thank Dr. James Thomas at the NIH Intramural

750 Sequencing Center (NISC) for his help with the PacBio sequencing. We would also like to thank

751 Dr. Gustav Paulay and Dr. Claudia Mills for their help navigating the complex taxonomy of

752 *Mnemiopsis*. Finally, we want to thank Dr. Mark Ravinet for his help brainstorming ideas

753 pertaining to the hybridization of these two species. ***Consent for Publication.*** The authors have

754 all been consulted on draft and final versions of the manuscript and have consented to

755 publication. ***Funding.*** This work was supported in part with a Postdoctoral Research Fellowship

in Biology (PRFB) from the National Science Foundation (award number: 2109712) to R.N.K, an Allen Distinguished Investigator Award from the Paul G. Allen Frontiers Group of the Paul G. Allen Family Foundation to J.F.R. This research was also supported in part by the Intramural Research Program of the National Human Genome Research Institute, National Institutes of Health (ZIA HG000140 to A.D.B). ***Data Availability.*** The datasets supporting the conclusions of this article are available at the NCBI under BioProject accession number PRJEB87530. The genome assemblies for each *Mnemiopsis* species are also available under the above BioProject accession codes. All scripts are publicly available at https://github.com/remiketchum/Mnemiopsis_2026. ***Authors' Contributions.*** Conceptualization: R.N.K and J.F.R. Investigation (fieldwork): R.N.K, W.B.L, E.G.S, J.F.R. Investigation (analysis): R.N.K, E.G.S, J.F.R, L.M.T, N.E.P. Resources: J.F.R, A.D.B, A.M.R. All authors read and approved the final manuscript. ***Competing Interests.*** Authors declare no competing interests. ***Ethics Approval and Consent to Participate.*** Not applicable.

Legends for Additional Files:

Additional File 1: Tables 1, 2, 4, 5, 7, 8, 10, 11, 12 and Figures 1-6.

Table S1 – Collection information for all samples collected along the US Atlantic coast including date of collection, number of samples collected, coordinates, and collection method.

Table S2 – Comparison of genome assembly benchmarks between the two published *Mnemiopsis leidyi* genomes and the two new genome assemblies.

Table S4 – F_{ST} values across all populations of *Mnemiopsis* collected based on the LD-Filtered SNP dataset.

Table S5 – f_3 results where each row represents a scenario where the FLP and MAW populations are the source for admixture and the third population is the target of hybridization. A f_3 statistic, the standard error (SE) and a Z-score value calculated with jackknife is provided for each scenario.

Table S7 – Gene Ontology (GO) analysis of genes in the top 1% regions of copy number variation outliers reveals enrichment in molecular functions (MF), cellular components (CC), and biological processes (BP).

Table S8 – Putative G protein-coupled receptors in the top 1% of copy number variation outliers.

Table S10 – Putative G-coupled protein receptors in the top 10% of XP-CLR outliers with corresponding *M. gardeni* gene ID.

Table S11 – Channels and receptors in the top 10% of XP-CLR outliers with corresponding *M. gardeni* gene ID.

Table S12 – Gene Ontology (GO) analysis of genes in the top 10% of XP-CLR outlier regions reveals enrichment in molecular functions, cellular components, and biological processes.

Figure S1 – Admixture plots for the 118 *Mnemiopsis* samples collected for K = 5 to K = 7 where each bar represents a single individual, and the colors represent each of the K components.

Figure S2 – Boxplots summarizing the best AIC scores for each model for all bootstrapped replicates for each of 102 demographic models tested. The inset plot shows the boxplot for the median AIC for the top ten best-fitting models in the set.

Figure S3 – Plots showing the goodness-of-fit of the best fitting model (sc3ielsm1). The top two panels show the observed AFS (top left) and the modeled AFS (top right). The

lower two plots show model errors plotted as residuals between the best-fit model and the data (bottom left) and the frequency histogram of residuals (bottom right).

Figure S4 – The best-fit demographic model (sc3ielsm1) inferred using *Moments* for the demographic history between *M. leidyi* and *M. gardeni*. This best-fit model includes three epochs in each species with symmetric migration in the first and asymmetric migration in the last.

Figure S5 – PCA plot based on copy number variation among samples. Copy number estimates were generated as denoised copy number ratios in GATK. Individuals are colored by their sampling location.

Figure S6 – The top V_{ST} outlier gene occurs in an *M. gardeni*-specific duplicated region. This dot plot shows BLAST hits (e-value < 1e-10; length >= 500bp) between corresponding regions in the *M. leidyi* and *M. gardeni* assemblies. The V_{ST} outlier gene (jg9426 – Mgar.v1.001:9329910-9331046) occurs as part of a larger duplicated region in *M. gardeni*. In *M. leidyi,* this region is single-copy. Arrows highlight the location of the *M. gardeni* duplicated genes.

Additional File 2: Table S3

Table S3 – Assembled gene/protein models that were annotated using three protein databases: UniProt Knowledgebase Swiss-Prot protein models v2021-03, RefSeq invertebrate protein models, and the *M. leidyi* protein models.

Additional File 3: Table S6

Table S6 – The top 1% of fixation index values (V_{ST}) for the copy number variation analyses with their associated annotations taken from Additional File 2: Table S3.

Additional File 4: Table S9

Table S9 – The top 10% of XP-CLR values calculated between the two lineages using a sliding window approach, a step-size of 10 Kb and the `maxSNPs flag` set to 200. We have appended their associated annotations from Additional File 2: Table S3.

References

1. Matute DR, Cooper BS. Comparative studies on speciation: 30 years since Coyne and Orr. Evol Int J Rrganic Evol. 2021;75:764–78. https://doi.org/10.1111/evo.14181.

2. Mayr E. Animal species and evolution. Harvard University Press; 1963.

3. Coyne JA, Orr HA. Speciation: a catalogue and critique of species concepts. Philos Biol Anthol. 2004;:272–92.

4. Frayer ME, Robles NV, Rodríguez-Barrera MJ, Coughlan JM, Schumer M. The molecular evolutionary basis of species formation revisited. Trends Genet. 2025;41:1068–95. https://doi.org/10.1016/j.tig.2025.07.003.

5. Bolnick DI, Fitzpatrick BM. Sympatric speciation: models and empirical evidence. Annu Rev Ecol Evol Syst. 2007;38:459–87.

6. Paudel Y, Madsen O, Megens H-J, Frantz LAF, Bosse M, Crooijmans RPMA, et al. Copy number variation in the speciation of pigs: a possible prominent role for olfactory receptors. BMC Genomics. 2015;16:330. https://doi.org/10.1186/s12864-015-1449-9.

7. Anderson SA, Weir JT. The role of divergent ecological adaptation during allopatric speciation in vertebrates. Science. 2022;378:1214–8.

8. De Jode A, Le Moan A, Johannesson K, Faria R, Stankowski S, Westram AM, et al. Ten years of demographic modelling of divergence and speciation in the sea. Evol Appl. 2023;16:542–59.

9. Palumbi SR. Genetic divergence, reproductive isolation, and marine speciation. Annu Rev Ecol Syst. 1994;:547–72.

10. Pogson GH. Studying the genetic basis of speciation in high gene flow marine invertebrates. Current Zoology. 2016;62:643–53.

11. Filatov DA. How does speciation in marine plankton work? Trends Microbiol. 2023;31:989–91. https://doi.org/10.1016/j.tim.2023.07.005.

12. Ravinet M, Faria R, Butlin RK, Galindo J, Bierne N, Rafajlović M, et al. Interpreting the genomic landscape of speciation: a road map for finding barriers to gene flow. Journal of Evolutionary Biology. 2017;30:1450–77.

13. Poikela N, Laetsch DR, Kankare M, Hoikkala A, Lohse K. Experimental introgression in Drosophila: asymmetric postzygotic isolation associated with chromosomal inversions and an incompatibility locus on the X chromosome. Mol Ecol. 2023;32:854–66.

14. Dettman JR, Anderson JB, Kohn LM. Divergent adaptation promotes reproductive isolation among experimental populations of the filamentous fungus Neurospora. BMC Evol Biol. 2008;8:35. https://doi.org/10.1186/1471-2148-8-35.

897 15. Dobzhansky T. Genetics and the origin of species. Columbia university press; 1982.

898 16. Foote AD. Sympatric speciation in the genomic era. Trends Ecol Evol. 2018;33:85–95.

899 17. White NJ, Snook RR, Eyres I. The Past and Future of Experimental Speciation. Trends Ecol
900 Evol. 2020;35:10–21. https://doi.org/10.1016/j.tree.2019.08.009.

901 18. Feder JL, Gejji R, Yeaman S, Nosil P. Establishment of new mutations under divergence and
902 genome hitchhiking. Philos Trans R Soc Lond B Biol Sci. 2012;367:461–74.
903 https://doi.org/10.1098/rstb.2011.0256.

904 19. Gavrilets S. Fitness landscapes and the origin of species. Princeton university press; 2004.

905 20. Michel AP, Sim S, Powell TH, Taylor MS, Nosil P, Feder JL. Widespread genomic
906 divergence during sympatric speciation. Proc Natl Acad Sci. 2010;107:9724–9.

907 21. Weissensteiner MH, Bunikis I, Catalán A, Francoijs K-J, Knief U, Heim W, et al. Discovery
908 and population genomics of structural variation in a songbird genus. Nat Commun.
909 2020;11:3403.

910 22. Davey JW, Chouteau M, Barker SL, Maroja L, Baxter SW, Simpson F, et al. Major
911 improvements to the Heliconius melpomene genome assembly used to confirm 10 chromosome
912 fusion events in 6 million years of butterfly evolution. G3 Genes Genomes Genet. 2016;6:695–
913 708.

914 23. Giménez MD, Förster DW, Jones EP, Jóhannesdóttir F, Gabriel SI, Panithanarak T, et al. A
915 half-century of studies on a chromosomal hybrid zone of the house mouse. J Hered.
916 2017;108:25–35.

917 24. Dierckxsens N, Li T, Vermeesch JR, Xie Z. A benchmark of structural variation detection by
918 long reads through a realistic simulated model. Genome Biol. 2021;22:1–16.

919 25. Zhang L, Reifová R, Halenková Z, Gompert Z. How important are structural variants for
920 speciation? Genes. 2021;12:1084.

921 26. Ferree PM, Barbash DA. Species-specific heterochromatin prevents mitotic chromosome
922 segregation to cause hybrid lethality in Drosophila. PLoS Biol. 2009;7:e1000234.

923 27. Ayala D, Guerrero RF, Kirkpatrick M. Reproductive isolation and local adaptation quantified
924 for a chromosome inversion in a malaria mosquito. Evolution. 2013;67:946–58.

925 28. Hager ER, Harringmeyer OS, Wooldridge TB, Theingi S, Gable JT, McFadden S, et al. A
926 chromosomal inversion contributes to divergence in multiple traits between deer mouse
927 ecotypes. Science. 2022;377:399–405.

928 29. Zuellig MP, Sweigart AL. Gene duplicates cause hybrid lethality between sympatric species
929 of Mimulus. PLoS Genet. 2018;14:e1007130.

930 30. Ho SS, Urban AE, Mills RE. Structural variation in the sequencing era. Nat Rev Genet.
931 2020;21:171–89.

932 31. Choo LQ, Spagliardi G, Malinsky M, Choquet M, Goetze E, Hoarau G, et al. Genome-wide
933 phylogeography reveals cryptic speciation in the circumglobal planktonic calcifier Limacina
934 bulimoides. Mol Ecol. 2023;32:3200–19.

935 32. Breusing C, Johnson SB, Tunnicliffe V, Clague DA, Vrijenhoek RC, Beinart RA. Allopatric
936 and Sympatric Drivers of Speciation in Alviniconcha Hydrothermal Vent Snails. Mol Biol Evol.
937 2020;37:3469–84. https://doi.org/10.1093/molbev/msaa177.

938 33. Schluter D, Howard DJ, Berlocher SH. Endless forms: species and speciation. Oxford Univ.
939 Press,; 1998.

940 34. Jaspers C, Costello JH, Colin SP. Carbon content of Mnemiopsis leidyi eggs and specific egg
941 production rates in northern Europe. J Plankton Res. 2015;37:11–5.

942 35. Shiganova T. Changes in appendicularian Oikopleura dioica abundance caused by invasion
943 of alien ctenophores in the Black Sea. J Mar Biol Assoc U K. 2005;85:477–94.

944 36. Ward RD, Woodwark M, Skibinski DOF. A comparison of genetic diversity levels in marine,
945 freshwater, and anadromous fishes. J Fish Biol. 1994;44:213–32.

946 37. Ketchum RN, Smith EG, DeBiasse MB, Vaughan GO, McParland D, Leach WB, et al.
947 Population genomic analyses of the sea urchin Echinometra sp. EZ across an extreme
948 environmental gradient. Genome Biol Evol. 2020;12:1819–29.

949 38. Knutsen H, Jorde PE, André C, Stenseth NC. Fine-scaled geographical population structuring
950 in a highly mobile marine species: the Atlantic cod. Mol Ecol. 2003;12:385–94.

951 39. Yan R-J, Schnabel KE, Rowden AA, Guo X-Z, Gardner JP. Population structure and genetic
952 connectivity of squat lobsters (Munida Leach, 1820) associated with vulnerable marine
953 ecosystems in the southwest Pacific Ocean. Front Mar Sci. 2020;6:791.

954 40. Kyle CJ, Boulding EG. Comparative population genetic structure of marine gastropods
955 (Littorina spp.) with and without pelagic larval dispersal. Mar Biol. 2000;137:835–45.

956 41. Mianzan HW, Martos P, Costello JH, Guerrero RA. Avoidance of hydrodynamically mixed
957 environments by Mnemiopsis leidyi (Ctenophora: Lobata) in open-sea populations from
958 Patagonia, Argentina. Jellyfish Blooms New Probl Solut. 2010;:113–24.

959 42. Harbison GR, Volovik SP. THE CTENOPHORE, MNEMIOPSIS LEIDYI, IN THE BLACK
960 SEA: A HOLOPLANKTONIC ORGANISM TRANSPORTED. In: Nonindigenous Estuarine &
961 Marine Organisms (NEMO): Proceedings of the Conference and Workshop, Seattle,
962 Washington, April 1993. US Department of Commerce, National Oceanic and Atmospheric
963 Administration; 1994. p. 25.

964 43. Mianzan HW, Martos P, Costello JH, Guerrero RA. Avoidance of hydrodynamically mixed
965 environments by Mnemiopsis leidyi (Ctenophora: Lobata) in open-sea populations from
966 Patagonia, Argentina. Jellyfish Blooms New Probl Solut. 2010;:113–24.

967 44. Lowe S, Browne M, Boudjelas S, De Poorter M. 100 of the world's worst invasive alien
968 species: a selection from the global invasive species database. Invasive Species Specialist Group
969 Auckland; 2000.

970 45. Doyle L. Mnemiopsis leidyi. Introd Mar INVASIVE SPECIES. 1984;52.

971 46. Shiganova TA. Adaptive strategies of Mnemiopsis leidyi A. Agassiz 1865 in different
972 environments of the Eurasian seas. Mar Pollut Bull. 2020;161:111737.

973 47. Jaspers C, Møller LF, Kiørboe T. Reproduction rates under variable food conditions and
974 starvation in Mnemiopsis leidyi: significance for the invasion success of a ctenophore. J Plankton
975 Res. 2015;37:1011–8.

976 48. Edgar A, Mitchell DG, Martindale MQ. Whole-body regeneration in the lobate ctenophore
977 Mnemiopsis leidyi. Genes. 2021;12:867.

978 49. Sasson DA, Ryan JF. The sex lives of ctenophores: the influence of light, body size, and self-
979 fertilization on the reproductive output of the sea walnut, Mnemiopsis leidyi. PeerJ.
980 2016;4:e1846.

981 50. Sasson DA, Jacquez AA, Ryan JF. The ctenophore Mnemiopsis leidyi regulates egg
982 production via conspecific communication. BMC Ecol. 2018;18:1–10.

983 51. Prentis PJ, Wilson JR, Dormontt EE, Richardson DM, Lowe AJ. Adaptive evolution in
984 invasive species. Trends Plant Sci. 2008;13:288–94.

985 52. Lee CE. Evolutionary genetics of invasive species. Trends Ecol Evol. 2002;17:386–91.

986 53. Child CM. The gradient in susceptibility to cyanides in the meridional conducting path of the
987 ctenophore Mnemiopsis. Am J Physiol-Leg Content. 1917;43:87–112.

988 54. Ryan JF, Pang K, Schnitzler CE, Nguyen A-D, Moreland RT, Simmons DK, et al. The
989 genome of the ctenophore Mnemiopsis leidyi and its implications for cell type evolution.
990 Science. 2013;342:1242592.

991 55. Moreland RT, Nguyen A-D, Ryan JF, Schnitzler CE, Koch BJ, Siewert K, et al. A
992 customized Web portal for the genome of the ctenophore Mnemiopsis leidyi. BMC Genomics.
993 2014;15:1–13.

994 56. Moreland RT, Nguyen A-D, Ryan JF, Baxevanis AD. The Mnemiopsis Genome Project
995 Portal: integrating new gene expression resources and improving data visualization. Database.
996 2020;2020:baaa029.

997 57. Moreland RT, Zhang S, Barreira SN, Ryan JF, Baxevanis AD. An AI-generated proteome-
998 scale dataset of predicted protein structures for the ctenophore Mnemiopsis leidyi. Proteomics.
999 2024;:2300397.

1000 58. Jaspers C, Ehrlich M, Pujolar JM, Künzel S, Bayer T, Limborg MT, et al. Invasion genomics
1001 uncover contrasting scenarios of genetic diversity in a widespread marine invader. Proc Natl
1002 Acad Sci. 2021;118:e2116211118.

1003 59. Bayha KM, Chang MH, Mariani CL, Richardson JL, Edwards DL, DeBoer TS, et al.
1004 Worldwide phylogeography of the invasive ctenophore Mnemiopsis leidyi (Ctenophora) based
1005 on nuclear and mitochondrial DNA data. Biol Invasions. 2015;17:827–50.

1006 60. Verwimp C, Vansteenbrugge L, Derycke S, Kerkhove T, Muylle H, Honnay O, et al.
1007 Population genomic structure of the gelatinous zooplankton species Mnemiopsis leidyi in its
1008 nonindigenous range in the North Sea. Ecol Evol. 2020;10:11–25.

1009 61. Reusch TB, Bolte S, Sparwel M, Moss AG, Javidpour J. Microsatellites reveal origin and
1010 genetic diversity of Eurasian invasions by one of the world's most notorious marine invader,
1011 Mnemiopsis leidyi (Ctenophora). Mol Ecol. 2010;19:2690–9.

1012 62. Pujolar JM, Breitburg D, Lee J, Decker MB, Jaspers C. Hybridization and adaptive
1013 introgression in a marine invasive species in native habitats. Iscience. 2023;26.

1014 63. Ahyong S, Boyko CB, Bernot J, Brandão SN, Daly M, De Grave S, et al. World Register of
1015 Marine Species (WoRMS). 2024.

1016 64. Seravin LN. The systematic revision of the genus Mnemiopsis (Ctenophora, Lobata). Zool Ž.
1017 1994;73:9–18.

1018 65. Manni M, Berkeley MR, Seppey M, Zdobnov EM. BUSCO: assessing genomic data quality
1019 and beyond. Curr Protoc. 2021;1:e323.

1020 66. Koutsouveli V, Torres-Oliva M, Bayer T, Fuß J, Grossschmidt N, Marulanda-Gomez AM, et
1021 al. The Chromosome-level Genome of the Ctenophore Mnemiopsis leidyi A. Agassiz, 1865
1022 Reveals a Unique Immune Gene Repertoire. Genome Biology and Evolution. 2025;17.

1023 67. Pett W, Ryan JF, Pang K, Mullikin JC, Martindale MQ, Baxevanis AD, et al. Extreme
1024 mitochondrial evolution in the ctenophore Mnemiopsis leidyi: Insight from mtDNA and the
1025 nuclear genome. Mitochondrial DNA. 2011;22:130–42.
1026 https://doi.org/10.3109/19401736.2011.624611.

1027 68. Toews DP, Brelsford A. The biogeography of mitochondrial and nuclear discordance in
1028 animals. Mol Ecol. 2012;21:3907–30.

1029 69. Skotte L, Korneliussen TS, Albrechtsen A. Estimating individual admixture proportions from
1030 next generation sequencing data. Genetics. 2013;195:693–702.

1031 70. Patterson N, Moorjani P, Luo Y, Mallick S, Rohland N, Zhan Y, et al. Ancient Admixture in
1032 Human History. Genetics. 2012;192:1065–93.

1033 71. Atağ G, Waldman S, Carmi S, Somel M. An explanation for the sister repulsion phenomenon
1034 in Patterson's f-statistics. Genetics. 2024;228:iyae144.

1035 72. Martin SH, Dasmahapatra KK, Nadeau NJ, Salazar C, Walters JR, Simpson F, et al.
1036 Genome-wide evidence for speciation with gene flow in Heliconius butterflies. Genome Res.
1037 2013;23:1817–28.

1038 73. Li M-R, Wang H-Y, Ding N, Lu T, Huang Y-C, Xiao H-X, et al. Rapid Divergence Followed
1039 by Adaptation to Contrasting Ecological Niches of Two Closely Related Columbine Species
1040 Aquilegia japonica and A. oxysepala. Genome Biology and Evolution. 2019;11:919–30.

1041 74. Liu X, Fu Y-X. Stairway Plot 2: demographic history inference with folded SNP frequency
1042 spectra. Genome Biol. 2020;21:280.

1043 75. Kleiven H (Kikki) F, Kissel C, Laj C, Ninnemann US, Richter TO, Cortijo E. Reduced North
1044 Atlantic deep water coeval with the glacial Lake Agassiz freshwater outburst. science.
1045 2008;319:60–4.

1046 76. Teller JT, Leverington DW, Mann JD. Freshwater outbursts to the oceans from glacial Lake
1047 Agassiz and their role in climate change during the last deglaciation. Quat Sci Rev.
1048 2002;21:879–87. https://doi.org/10.1016/S0277-3791(01)00145-7.

1049 77. Martínez-García L, Ferrari G, Oosting T, Ballantyne R, Van der Jagt I, Ystgaard I, et al.
1050 Historical demographic processes dominate genetic variation in ancient Atlantic cod
1051 mitogenomes. Front Ecol Evol. 2021;9:671281.

1052 78. Atmore LM, Martínez-García L, Makowiecki D, André C, Lõugas L, Barrett JH, et al.
1053 Population dynamics of Baltic herring since the Viking Age revealed by ancient DNA and
1054 genomics. Proc Natl Acad Sci. 2022;119:e2208703119.

1055 79. Li H, Durbin R. Inference of human population history from individual whole-genome
1056 sequences. Nature. 2011;475:493–6.

1057 80. Liu X, Fu Y-X. Exploring population size changes using SNP frequency spectra. Nat Genet.
1058 2015;47:555–9.

1059 81. Jouganous J, Long W, Ragsdale AP, Gravel S. Inferring the Joint Demographic History of
1060 Multiple Populations: Beyond the Diffusion Approximation. Genetics. 2017;206:1549–67.

1061 82. Prada C, Hellberg ME. Speciation-by-depth on coral reefs: Sympatric divergence with gene
1062 flow or cryptic transient isolation? Journal of Evolutionary Biology. 2021;34:128–37.

1063 83. Putnam NH, Srivastava M, Hellsten U, Dirks B, Chapman J, Salamov A, et al. Sea anemone
1064 genome reveals ancestral eumetazoan gene repertoire and genomic organization. science.
1065 2007;317:86–94.

1066 84. Putnam NH, Butts T, Ferrier DE, Furlong RF, Hellsten U, Kawashima T, et al. The
1067 amphioxus genome and the evolution of the chordate karyotype. Nature. 2008;453:1064–71.

1068 85. Simakov O, Marletaz F, Cho S-J, Edsinger-Gonzales E, Havlak P, Hellsten U, et al. Insights
1069 into bilaterian evolution from three spiralian genomes. Nature. 2013;493:526–31.

1070 86. Schultz DT, Haddock SH, Bredeson JV, Green RE, Simakov O, Rokhsar DS. Ancient gene
1071 linkages support ctenophores as sister to other animals. Nature. 2023;618:110–7.

1072 87. Lewin TD, Liao IJ-Y, Luo Y-J. Annelid comparative genomics and the evolution of massive
1073 lineage-specific genome rearrangement in bilaterians. Mol Biol Evol. 2024;41:msae172.

1074 88. Johnson SB, Winnikoff JR, Schultz DT, Christianson LM, Patry WL, Mills CE, et al.
1075 Speciation of pelagic zooplankton: Invisible boundaries can drive isolation of oceanic
1076 ctenophores. Front Genet. 2022;13:970314.

1077 89. Mérot C, Oomen RA, Tigano A, Wellenreuther M. A roadmap for understanding the
1078 evolutionary significance of structural genomic variation. Trends Ecol Evol. 2020;35:561–72.

1079 90. O'Neill MJ, O'Neill RJ. Sex chromosome repeats tip the balance towards speciation. Mol
1080 Ecol. 2018;27:3783–98.

1081 91. Hull RM, Cruz C, Jack CV, Houseley J. Environmental change drives accelerated adaptation
1082 through stimulated copy number variation. PLoS Biol. 2017;15:e2001333.

1083 92. Ashburner M, Ball CA, Blake JA, Botstein D, Butler H, Cherry JM, et al. Gene ontology:
1084 tool for the unification of biology. Nat Genet. 2000;25:25–9.

1085 93. Babonis LS, Martindale MQ, Ryan JF. Do novel genes drive morphological novelty? An
1086 investigation of the nematosomes in the sea anemone Nematostella vectensis. BMC Evol Biol.
1087 2016;16:114. https://doi.org/10.1186/s12862-016-0683-3.

1088 94. Schluter D. Evidence for ecological speciation and its alternative. Science. 2009;323:737–41.

1089 95. Carruthers M, Carleton KL, Linderoth T, Bridle J, Hudson AG, Malinsky M, et al. Rapid
1090 Divergence of Visual Systems and Signaling Traits to Contrasting Light Regimes During Early
1091 Speciation of African Crater Lake Cichlid Fish. Mol Biol Evol. 2025;42:msaf204.

1092 96. Klein J, Ono H, Klein D, O'hUigin C. The accordion model of MHC evolution. In: Progress
1093 in Immunology Vol. VIII. Springer; 1993. p. 137–43.

1094 97. Secomandi S, Gallo GR, Rossi R, Rodríguez Fernandes C, Jarvis ED, Bonisoli-Alquati A, et
1095 al. Pangenome graphs and their applications in biodiversity genomics. Nat Genet. 2025;57:13–
1096 26. https://doi.org/10.1038/s41588-024-02029-6.

1097 98. Sirén J, Monlong J, Chang X, Novak AM, Eizenga JM, Markello C, et al. Pangenomics
1098 enables genotyping of known structural variants in 5202 diverse genomes. Science.
1099 2021;374:abg8871.

1100 99. Chen H, Patterson N, Reich D. Population differentiation as a test for selective sweeps.
1101 Genome Res. 2010;20:393–402.

1102 100. Torres C-R, Hart GW. Topography and polypeptide distribution of terminal N-
1103 acetylglucosamine residues on the surfaces of intact lymphocytes. Evidence for O-linked
1104 GlcNAc. J Biol Chem. 1984;259:3308–17.

1105 101. Guo B, Liang Q, Li L, Hu Z, Wu F, Zhang P, et al. O-GlcNAc-modification of SNAP-29
1106 regulates autophagosome maturation. Nat Cell Biol. 2014;16:1215–26.
1107 https://doi.org/10.1038/ncb3066.

1108 102. Mizushima N. Sugar modification inhibits autophagosome–lysosome fusion. Nat Cell Biol.
1109 2014;16:1132–3. https://doi.org/10.1038/ncb3078.

1110 103. Morinaga G, Balcazar D, Badolo A, Iyaloo D, Tantely L, Mouillaud T, et al. From macro to
1111 micro: De novo genomes of Aedes mosquitoes enable comparative genomics among close and
1112 distant relatives. bioRxiv. 2025;:2025.01. 13.632753.

1113 104. MacGuigan DJ, Krabbenhoft TJ, Harrington RC, Wainwright DK, Backenstose NJC, Near
1114 TJ. Lacustrine speciation associated with chromosomal inversion in a lineage of riverine fishes.
1115 Evolution. 2023;77:1505–21.

1116 105. Wu N, Evans E, van Schooten B, Meléndez-Rosa J, Ortiz Y, Planas Soto-Navarro SM, et al.
1117 Widespread Gene Expression Divergence in Butterfly Sensory Tissues Plays a Fundamental
1118 Role During Reproductive Isolation and Speciation. Molecular Biology and Evolution. 2022;39.

1119 106. Yoshida K, Rödelsperger C, Röseler W, Riebesell M, Sun S, Kikuchi T, et al. Chromosome
1120 fusions repatterned recombination rate and facilitated reproductive isolation during Pristionchus
1121 nematode speciation. Nat Ecol Evol. 2023;7:424–39.

1122 107. Ehrlich M. Invasion Genomics: population structure and diversity patterns in the invasive
1123 ctenophore Mnemiopsis leidyi based on whole-genome re-sequencing. Christian-Albrechts-
1124 Universität Kiel; 2017.

1125 108. Cheng H, Concepcion GT, Feng X, Zhang H, Li H. Haplotype-resolved de novo assembly
1126 using phased assembly graphs with hifiasm. Nat Methods. 2021;18:170–5.

1127 109. Roach MJ, Schmidt SA, Borneman AR. Purge Haplotigs: allelic contig reassignment for
1128 third-gen diploid genome assemblies. BMC Bioinformatics. 2018;19:1–10.

1129 110. Flynn JM, Hubley R, Goubert C, Rosen J, Clark AG, Feschotte C, et al. RepeatModeler2 for
1130 automated genomic discovery of transposable element families. Proc Natl Acad Sci.
1131 2020;117:9451–7.

1132 111. Babonis LS, DeBiasse MB, Francis WR, Christianson LM, Moss AG, Haddock SH, et al.
1133 Integrating embryonic development and evolutionary history to characterize tentacle-specific cell
1134 types in a ctenophore. Mol Biol Evol. 2018;35:2940–56.

1135 112. Langmead B, Salzberg SL. Fast gapped-read alignment with Bowtie 2. Nat Methods.
1136 2012;9:357–9.

1137 113. Brůna T, Hoff KJ, Lomsadze A, Stanke M, Borodovsky M. BRAKER2: automatic
1138 eukaryotic genome annotation with GeneMark-EP+ and AUGUSTUS supported by a protein
1139 database. NAR Genomics Bioinforma. 2021;3:lqaa108.

1140 114. Buchfink B, Reuter K, Drost H-G. Sensitive protein alignments at tree-of-life scale using
1141 DIAMOND. Nat Methods. 2021;18:366–8.

1142 115. El Hilali S, Copley RR. macrosyntR: Drawing automatically ordered Oxford Grids from
1143 standard genomic files in R. bioRxiv. 2023;:2023.01. 26.525673.

1144 116. Babadi M, Fu JM, Lee SK, Smirnov AN, Gauthier LD, Walker M, et al. GATK-gCNV
1145 enables the discovery of rare copy number variants from exome sequencing data. Nat Genet.
1146 2023;55:1589–97.

1147 117. Marçais G, Delcher AL, Phillippy AM, Coston R, Salzberg SL, Zimin A. MUMmer4: A
1148 fast and versatile genome alignment system. PLoS Comput Biol. 2018;14:e1005944.

1149 118. Goel M, Sun H, Jiao W-B, Schneeberger K. SyRI: finding genomic rearrangements and
1150 local sequence differences from whole-genome assemblies. Genome Biol. 2019;20:1–13.

1151 119. Goel M, Schneeberger K. Plotsr: visualizing structural similarities and rearrangements
1152 between multiple genomes. Bioinformatics. 2022;38:2922–6.

1153 120. Li H, Handsaker B, Wysoker A, Fennell T, Ruan J, Homer N, et al. The sequence
1154 alignment/map format and SAMtools. bioinformatics. 2009;25:2078–9.

1155 121. Bolger AM, Lohse M, Usadel B. Trimmomatic: a flexible trimmer for Illumina sequence
1156 data. Bioinformatics. 2014;30:2114–20.

1157 122. Tarasov A, Vilella AJ, Cuppen E, Nijman IJ, Prins P. Sambamba: fast processing of NGS
1158 alignment formats. Bioinformatics. 2015;31:2032–4.

1159 123. Jun G, Wing MK, Abecasis GR, Kang HM. An efficient and scalable analysis framework
1160 for variant extraction and refinement from population-scale DNA sequence data. Genome Res.
1161 2015;25:918–25.

1162 124. Korneliussen TS, Albrechtsen A, Nielsen R. ANGSD: analysis of next generation
1163 sequencing data. BMC Bioinformatics. 2014;15:1–13.

1164 125. Fox EA, Wright AE, Fumagalli M, Vieira FG. ngsLD: evaluating linkage disequilibrium
1165 using genotype likelihoods. Bioinformatics. 2019;35:3855–6.

1166 126. Lou RN, Jacobs A, Wilder AP, Therkildsen NO. A beginner's guide to low-coverage whole
1167 genome sequencing for population genomics. Mol Ecol. 2021;30:5966–93.

1168 127. Nei M, Li W-H. Mathematical model for studying genetic variation in terms of restriction
1169 endonucleases. Proc Natl Acad Sci. 1979;76:5269–73.

1170 128. Tajima F. Statistical method for testing the neutral mutation hypothesis by DNA
1171 polymorphism. Genetics. 1989;123:585–95.

1172 129. Fumagalli M, Vieira FG, Linderoth T, Nielsen R. ngsTools: methods for population
1173 genetics analyses from next-generation sequencing data. Bioinformatics. 2014;30:1486–7.

1174 130. Lefort V, Desper R, Gascuel O. FastME 2.0: a comprehensive, accurate, and fast distance-
1175 based phylogeny inference program. Mol Biol Evol. 2015;32:2798–800.

1176 131. Kozlov AM, Darriba D, Flouri T, Morel B, Stamatakis A. RAxML-NG: a fast, scalable and
1177 user-friendly tool for maximum likelihood phylogenetic inference. Bioinformatics.
1178 2019;35:4453–5.

1179 132. Letunic I, Bork P. Interactive Tree of Life (iTOL) v6: recent updates to the phylogenetic
1180 tree display and annotation tool. Nucleic Acids Res. 2024;:gkae268.

1181 133. Dierckxsens N, Mardulyn P, Smits G. NOVOPlasty: de novo assembly of organelle
1182 genomes from whole genome data. Nucleic Acids Res. 2017;45:e18–e18.

1183 134. Ghabooli S, Shiganova TA, Briski E, Piraino S, Fuentes V, Thibault-Botha D, et al.
1184 Invasion pathway of the ctenophore Mnemiopsis leidyi in the Mediterranean Sea. PloS One.
1185 2013;8:e81067.

1186 135. Christianson LM, Johnson SB, Schultz DT, Haddock SH. Hidden diversity of Ctenophora
1187 revealed by new mitochondrial COI primers and sequences. Mol Ecol Resour. 2022;22:283–94.

1188 136. Ayad LA, Pissis SP. MARS: improving multiple circular sequence alignment using refined
1189 sequences. BMC Genomics. 2017;18:1–10.

1190 137. Katoh K, Standley DM. MAFFT multiple sequence alignment software version 7:
1191 improvements in performance and usability. Mol Biol Evol. 2013;30:772–80.

1192 138. Minh BQ, Schmidt HA, Chernomor O, Schrempf D, Woodhams MD, Von Haeseler A, et
1193 al. IQ-TREE 2: new models and efficient methods for phylogenetic inference in the genomic era.
1194 Mol Biol Evol. 2020;37:1530–4.

1195 139. Presnell JS, Bubel M, Knowles T, Patry W, Browne WE. Multigenerational laboratory
1196 culture of pelagic ctenophores and CRISPR–Cas9 genome editing in the lobate Mnemiopsis
1197 leidyi. Nat Protoc. 2022;17:1868–900. https://doi.org/10.1038/s41596-022-00702-w.

1198 140. Edgar A, Ponciano JM, Martindale MQ. Ctenophores are direct developers that reproduce
1199 continuously beginning very early after hatching. Proc Natl Acad Sci. 2022;119:e2122052119.

1200 141. Rippe JP, Dixon G, Fuller ZL, Liao Y, Matz M. Environmental specialization and cryptic
1201 genetic divergence in two massive coral species from the Florida Keys Reef Tract. Mol Ecol.
1202 2021;30:3468–84.

1203 142. Quinlan AR, Hall IM. BEDTools: a flexible suite of utilities for comparing genomic
1204 features. Bioinformatics. 2010;26:841–2.

1205